Sensitivity study of D_s particle in Belle

Deepanshu

A dissertation submitted for the partial fulfilment of BS-MS dual degree in Science

Indian Institute of Science Education and Research Mohali
July 2017

Certificate of Examination

This is to certify that the dissertation titled "Sensitivity study of D_s particle in Belle submitted" by Deepanshu (Reg. No. MS11020) for the partial fulfilment of BS-MS dual degree programme of the Institute, has been examined by the thesis committee duly appointed by the Institute. The committee finds the work done by the candidate satisfactory and recommends that the report be accepted.

Dr. Harvinder Kaur Jassal Dr. Satyajit Jena Dr. Vishal Bhardwaj
(Supervisor)

Declaration

The work presented in this dissertation has been carried out by me under the guidance of Dr. Vishal Bhardwaj at the Indian Institute of Science Education and Research Mohali.
This work has not been submitted in part or in full for a degree, a diploma, or a fellowship to any other university or institute. Whenever contributions of others are involved, every effort is made to indicate this clearly, with due acknowledgement of collaborative research and discussions. This thesis is a bonafide record of work done by me and all sources listed within have been detailed in the bibliography.

Deepanshu

(Candidate)

Dated: July 17, 2017

In my capacity as the supervisor of the candidate's project work, I certify that the above statements by the candidate are true to the best of my knowledge.

Dr. Vishal Bhardwaj
(Supervisor)

Acknowledgement

I would first like to thank my thesis advisor Dr. Vishal Bhardwaj and want to express my sincere gratitude towards him for the continuous support of my Master's thesis related research, for his patience, motivation, and immense knowledge. His guidance helped me in all the time of research and writing of this thesis. I could not have imagined having a better advisor and mentor for my Master's thesis. The door to Dr. Bhardwaj office was always open whenever I ran into a trouble spot or had a question about my research or writing. He consistently allowed this thesis to be my own work, but steered me in the right the direction whenever he thought I needed it.

I would also like to thank the experts who were involved in the validation survey for this research project: Dr. Harvinder Kaur Jassal and Dr. Satyajit Jena. Without their passionate participation and input, the validation survey could not have been successfully conducted.

Finally, I must express my very profound gratitude to my parents, my sister and my friends: Supreet Kaur, Jagdeep Singh, Samridhi Gambhir, Abhimanyu Bhardwaj, Shubham Anand, Jasmeet Singh, and Mandisha Saini for providing me with unfailing support and continuous encouragement throughout my years of study and through the process of researching and writing this thesis. This accomplishment would not have been possible without them.

Thank you.

Abstract

We know that Standard Model has shortcomings and we need New Physics beyond the Standard Model to explain those shortcomings. D_s radiative decays may provide an opportunity to search for New Physics. In this MS thesis work, the feasibility study was done for $D_s^{\pm} \to \rho^{\pm}\gamma$ and $D_s^{\pm} \to K^{*\pm}\gamma$ decays using Belle data was done for the first time. Belle detector was located at an interaction point of the KEKB asymmetric-energy $e^+ e^-$ collider (i.e. 8 GeV and 3.5 GeV respectively) at High Energy Accelerator Research Organisation, KEK, Japan. As of now, it is being upgraded to Belle II detector. Belle Collaboration has collected large set of data at $\Upsilon(4S)$ resonance. Along with this it also has large data collection of charm mesons. We generated signal MC sample using EvtGen. In order to identify D_s mesons, we used tagging method using $D_s^* \rightarrow D_s\gamma$. This helps in reduction of the background. To further reduce the background coming from the soft energy photons, we use π^0 veto, momentum of D_s^* in centre of mass frame. I also prepared skimming sample which can be used later on for this study.

Content

Chapter-1

Introduction

1.1 The Standard Model

Standard Model (SM) of particle physics, as per our present knowledge, describes the Universe in terms of matter (fermions) and force (bosons). Fermions contain leptons and quarks that are the building blocks of matter and the interaction between these particles are mediated by bosons. So, the matter is made out of three kinds of "elementary particles" i.e., leptons, quarks, and mediators. [1]

The SM includes 12 elementary particles of spin ½ i.e. fermions. There are six quarks (up, down, charm, strange, top, and bottom), and six leptons (electron, electron neutrino, muon, muon neutrino, tau, and tau neutrino). Pairs from each classification are grouped together to form a generation, with corresponding particles exhibiting similar physical behaviour. There are three generations of fermions and are depicted in Table 1.1.

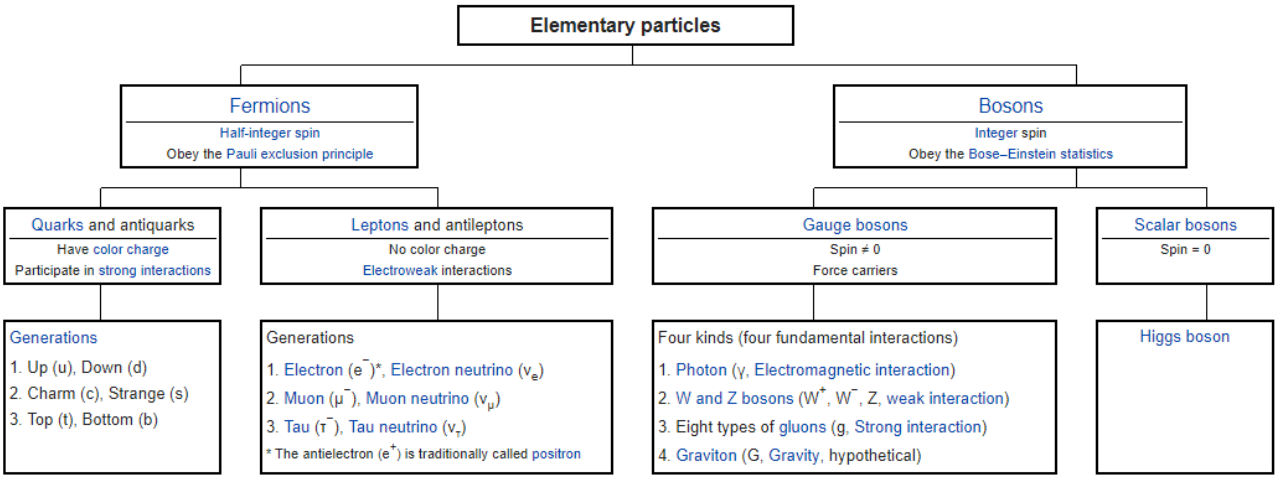

Table 1.1: Classes of elementary particles of the SM [Source: *Wikipedia*].

Bosons are particles having an integer spin (0, 1, 2, …) and act as force carriers that mediate the strong, weak, gravitational (not in SM) and electromagnetic interactions which is shown in Table 2. Photons being massless, mediate the electromagnetic force between electrically charged particles, W^+, W^-, and Z bosons mediate the weak interactions between particles of different flavours (all quarks and leptons) as Z is more massive than $W^\pm$. The weak interactions involving the $W^\pm$ exclusively act on left-handed particles and right-handed antiparticles. Also, $W^\pm$ carry an electric charge of +1 and −1 and couple to the electromagnetic interaction. The electrically neutral Z boson interacts with both left-handed particles and antiparticles. These three bosons along with the photons are grouped together and collectively mediate the electroweak interactions. Another type of mediator is the 'eight gluons' which mediate the strong interactions between color charged particles (quarks). Gluons are massless, they have an effective color charge and they can also interact amongst themselves, even in the presence of a quark. This is the reason due to which the isolated gluon and quark are difficult to observe in the experiments directly.

Property/Interaction	Gravitation	Weak	Electromagnetic	Strong	
		(Electroweak)		Fundamental	Residual
Acts on:	Mass - Energy	Flavor	Electric charge	Color charge	Atomic nuclei
Particles experiencing:	All	Quarks, leptons	Electrically charged	Quarks, Gluons	Hadrons
Particles mediating:	Not yet observed (Graviton hypothesised)	W^+, W^- and Z^0	γ (photon)	Gluons	π, ρ and ω mesons
Strength at the scale of quarks:	10^{-41}	10^{-4}	1	60	Not applicable to quarks
Strength at the scale of protons/neutrons:	10^{-36}	10^{-7}	1	Not applicable to hadrons	20

Table 1.2: The four fundamental interactions of nature [Source: *Wikipedia*].

1.1.1 Is Standard Model complete?

Despite being the most successful and interesting theory of particle physics, the SM is not perfect. There are fundamental physical phenomena in nature that the SM does not adequately explain. For example: '*Neutrino masses'*-According to the SM, neutrinos are massless particles but Neutrino Oscillation experiments have shown that neutrinos do have mass; '*Gravity'*- The SM does not explain gravity and it is widely considered to be incompatible with the most successful theory of gravity to date i.e. General Relativity. Similarly, there are many other physical phenomena, experiments and theoretical predictions that are not in terms with the SM. Hence, there is a need for New Physics 'NP' that would modify the SM in ways subtle enough to be consistent with the existing data. [2]

1.2 Mesons

Because of the color confinement phenomenon in quarks they are very strongly bound to one another, forming color-neutral composite particles (hadrons), containing a quark and an antiquark, which is basically a meson. The other member of hadron family is baryon- subatomic particle composed of three quarks. The main difference between both of them is that baryon has spin ½ i.e. it is a fermion and meson has an integer spin i.e. it is a boson. [3]

They are composed of quarks hence both weak and strong interactions are feasible in case of mesons. Mesons with electric charge can also participate in electromagnetic interactions that are classified by quark content, total angular momentum, parity, *C* parity, iso-spin and charge and many more properties. They are also typically less massive than baryons, which means that they are more easily produced in experiments, and will exhibit higher-energy phenomena sooner than baryons would. For example, the charm quark was first seen in the J/Psi meson (J/ψ) in 1974, and the bottom quark in the upsilon meson (Υ) in 1977.

1.2.1 Spin, Orbital and total Angular momentum

Spin quantum number (S) is a vector quantity that represents the 'intrinsic' angular momentum of a particle. It comes in increments of ½ $\hbar$. Quarks have spin ½ (S=½), a single quark has a spin vector of length½, and two spin projections (S_Z=+½ and S_Z=−½). When two quarks have their spins aligned, their two spin vectors add to make a vector of length S=1 whereas in case of three spin projections (S_Z=+1, S_Z=0, and S_Z=−1), if two quarks have unaligned spins, the spin vectors add up to make a vector of length S=0 with only one spin projection (S_Z=0), called the spin-0 singlet. Because mesons are made of one quark and one antiquark, they can be found in both triplet and singlet spin states.

There is another quantity of angular momentum, called the orbital angular momentum (quantum number L), which represents the angular momentum due to quarks orbiting around each other. The total angular momentum (quantum number J) of a particle is therefore the combination of intrinsic angular momentum (S) and orbital angular momentum (L). It can take any value from $J = |L - S|$ to $J = |L + S|$, in increments of 1.

1.2.2 Parity

If the universe was reflected in a mirror, most of the laws of physics would be identical: things would behave the same way regardless of what we call ‘left’ and what we call ‘right’. This concept of mirror reflection is called parity (*P*) i.e. if the quantum field for each particle is mirror-reversed, then the new set of wave function will satisfy the laws of physics.

Gravity (the electromagnetic force) and the strong interactions, all behave in the same way as they are said to conserve parity (*P*-symmetry). However, the weak interactions do distinguish ‘left’ from ‘right’, a phenomenon called parity violation (*P*-violation).

For mesons: *P* is related to orbital *L* by the relation $P = (-1)^{(L+1)}$. The '+1' in the exponent comes from the Dirac equation: a quark and an antiquark have opposite intrinsic parities. Therefore, mesons with no orbital angular momentum (L=0) have odd parity (P= −1).

1.2.3 *C* parity

This property is only defined for mesons that are their own antiparticles (i.e. neutral mesons). It represents whether or not the wave function of the meson remains the same under the interchange of their quark with their antiquark.

If *C* is +1 then it is even and if *C* is -1 then it is odd.

C parity is studied rarely on its own, but more commonly in combination with *P* parity i.e. *CP* parity. *CP* parity was thought to be conserved, but was later found to be violated in weak interactions.

1.3 Charm meson

In 1976, the *D* mesons were discovered by the Mark I detector at the Stanford Linear Accelerator Centre. Since they are the lightest mesons containing a single charm quark or antiquark, they must change the charm (anti)quark into an (anti)quark of another type to decay.

Such transitions take place only via weak interactions and involve a change of the internal charm quantum number. In *D* mesons, the charm quark preferentially

changes into a strange quark via an exchange of a *W* particle, therefore they preferentially decay into kaons and pions. [4]

Particle	Symbol	Anti-particle	Makeup	Rest mass (MeV/c^2)	*S*	*C*	Lifetime (s)
D	D^+	D^-	c$\underline{\text{d}}$	1869.4	0	+1	10.6×10^{-13}
D	D^0	D^0	c$\underline{\text{u}}$	1864.6	0	+1	4.2×10^{-13}
D	D_s^+	D_s^-	c$\underline{\text{s}}$	1969.0	+1	+1	4.7×10^{-13}

1.3.1 Why we choose D_s?

In SM, the physics of charm meson is not expected to have NP discovery potential because the relevant Cabibbo-Kobayashi-Maskawa matrix elements V_{cs} *and* V_{cd} are well known, *CP* asymmetries and D^0 – D^0 oscillations are small. Further, the weak decays of *D* mesons are also difficult to investigate due to the strong final state interactions, and its rare decays are expected to have very small branching ratios. However, it has been pointed that the oscillations and $c \rightarrow u\gamma$ decays might have some contributions coming from the non-minimal super symmetry (which is NP scenario). Therefore, one can search for NP using $c \rightarrow u\gamma$ transitions. It was suggested that NP will result in deviation from

$$R_{\rho/\omega} \equiv \frac{\Gamma(D^0 \rightarrow \rho^0/\omega\,\gamma)}{\Gamma(D^0 \rightarrow \bar{K}^{*0}\gamma)} = \frac{\tan^2\theta_C}{2} \qquad (1)$$

B. Bajc *et al* [5] studied Cabibbo suppressed D^0, D^+, D_s^+ radiative weak decays in order to find the best mode to test $c \rightarrow u\gamma$ decay. They calculated the ratios between various Cabibbo suppressed and Cabibbo allowed charm meson radiative weak decays, as predicted by the SM. After analysing them they noticed that the equation (1) can be violated already in the SM framework (because of large, unknown correction within SM) while a similar relation for D_S^+ radiative decays offers a much better test for $c \rightarrow u\gamma$

$$R_K \equiv \frac{\Gamma(D_s^+ \to K^{*+}\gamma)}{\Gamma(D_s^+ \to \rho^+\gamma)} = \tan^2\theta_C \qquad (2)$$

Further radiative D_S decays, such as $D_S^+ \to K^{*+}\gamma$ and $D_S^+ \to \rho^+\gamma$, have not been observed yet. So, for us the first step is to measure its branching fraction. In this master thesis, we tried to come up with basics selection criteria for the signal identification. Further, we studied the potential background and identified the variables one can exploit in order to suppress it.

1.3.2 Decay Modes taken for this thesis

In this MS thesis work, we deal with three kinds of decay modes and have generated one million signal MC entries for each mode.

Mode 1:

$$D_s^+ \to \rho^+\gamma \quad \text{where } \rho^+ \to \pi^+\pi^0$$

$$D_s^- \to \rho^-\gamma \quad \text{where } \rho^- \to \pi^-\pi^0$$

Mode2:

$$D_s^+ \to K^{*+}\gamma \quad \text{where } K^{*+} \to \pi^+ K_s$$

$$D_s^- \to K^{*-}\gamma \quad \text{where } K^{*-} \to \pi^- K_s$$

Mode3:

$$D_s^+ \to K^{*+}\gamma \quad \text{where } K^{*+} \to \pi^0 K^+$$

$$D_s^- \to K^{*-}\gamma \quad \text{where } K^{*-} \to \pi^0 K^-$$

Branching Fraction (world average by PDG):

$$\rho^+ \to \pi^+\pi^0 \qquad BF = 100\%$$

$$K^{*+} \to \pi^+ K_s \qquad BF = 33.3\%$$

$$K^{*+} \to \pi^0 K^+ \qquad BF = 33.3\%$$

Chapter-2

Belle Experimental Setup

The work done in this thesis has simulated the data using the Belle detector environment. Belle detector was located at an interaction point of the KEKB asymmetric-energy e^+ e^- collider at High Energy Accelerator Research Organisation, KEK, Japan. The Belle detector was designed and optimized to carry out a suite of measurements in various decay modes of *B* mesons to verify the Kobayashi-Maskawa mechanism that explains *CP* violation in the SM. Major part of the data has been accumulated at the $\Upsilon(4S)$ resonance in order to record as many *B* mesons as possible for the above *CP* violation study. However, the KEKB beam energies are tuneable enabling Belle to collect data at $\Upsilon(1S)$, $\Upsilon(2S)$, $\Upsilon(3S)$ and $\Upsilon(5S)$ resonances. Besides these, Belle has accumulated a copious amount of *D* mesons at various $\Upsilon(nS)$ resonances for studying charm physics. Not only it is a *B*-factory, but also eligible to be called a *D*-factory.

2.1 KEKB

The KEK *B*-Factory (KEKB) is a two-ring, asymmetric energy e^+ e^- collider, The KEKB achieved its highest peak luminosity, $2.1\times10^{34}cm^{-2}$ s^{-1} during June 2009 that was more than twice the design value ($1\times10^{34}cm^{-2}$ s^{-1}). As a result, Belle was able to accumulate over 1 ab^{-1} of data. An 8GV electron ring (High Energy Ring) and a 3.5GeV positron ring (Low Energy Ring) are installed side by side in a tunnel 11m below the ground level, as shown in Fig.2.1. Both rings are about 3km long and can store beam currents up to 2.0A in the LER and 1.35A in the HER with 508.9 MHz radio frequency (RF) acceleration systems. The two beams collide at the interaction point (IP) with a finite angle of 22 mrad in the horizontal plane. The nonzero crossing angle allows to fill all RF buckets with bunches without any risk of parasitic collision. The crossing angle also eliminates the need for separation dipole magnet at

an expense of lower luminosity. In order to compensate the loss in luminosity, two super conducting crab cavities were installed in each ring. In crab the crossing scheme, the bunches are kicked in the horizontal plane by transverse RF in the crab cavities so that they rotate and collide head-on at the IP.

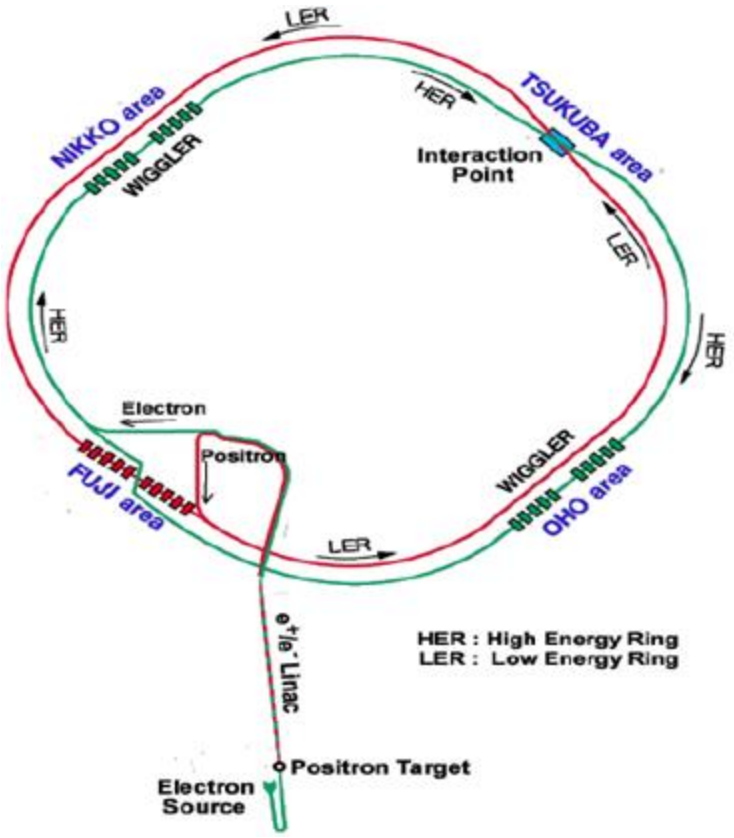

Figure 2.1: Schematic view of the KEKB collider

2.2 Belle Detector

The Belle detector is constructed to carry out quantitative study of *B*-meson decays especially the rare *B* decay modes with very small branching fractions. *B* mesons are very short-lived particles and decay instantaneously into relatively longlife time particles before they reach the innermost part of the detector. Belle detector detects the particles namely $e^{\pm}$, $\mu^{\pm}$, $\pi^{\pm}$, $K^{\pm}$, p, $\underline{p}$, γ and K^{0}. The neutron and anti-neutron which are produced cannot be detected.

Belle consists of concentric layers of sub-detectors designed to provide momentum and position information via magnetic spectroscopy, energy measurements via electromagnetic calorimeter, and particle identification through energy loss and penetration depth data. The sub-detectors are:

- Silicon vertex detector (SVD)
- Central drift chamber (CDC)
- Aerogel Cerenkov counter (ACC)
- Time of flight scintillator (TOF)
- Electromagnetic calorimeter (ECL)
- Kaon and muon detector (KLM)
- Extreme forward calorimeter (EFC)

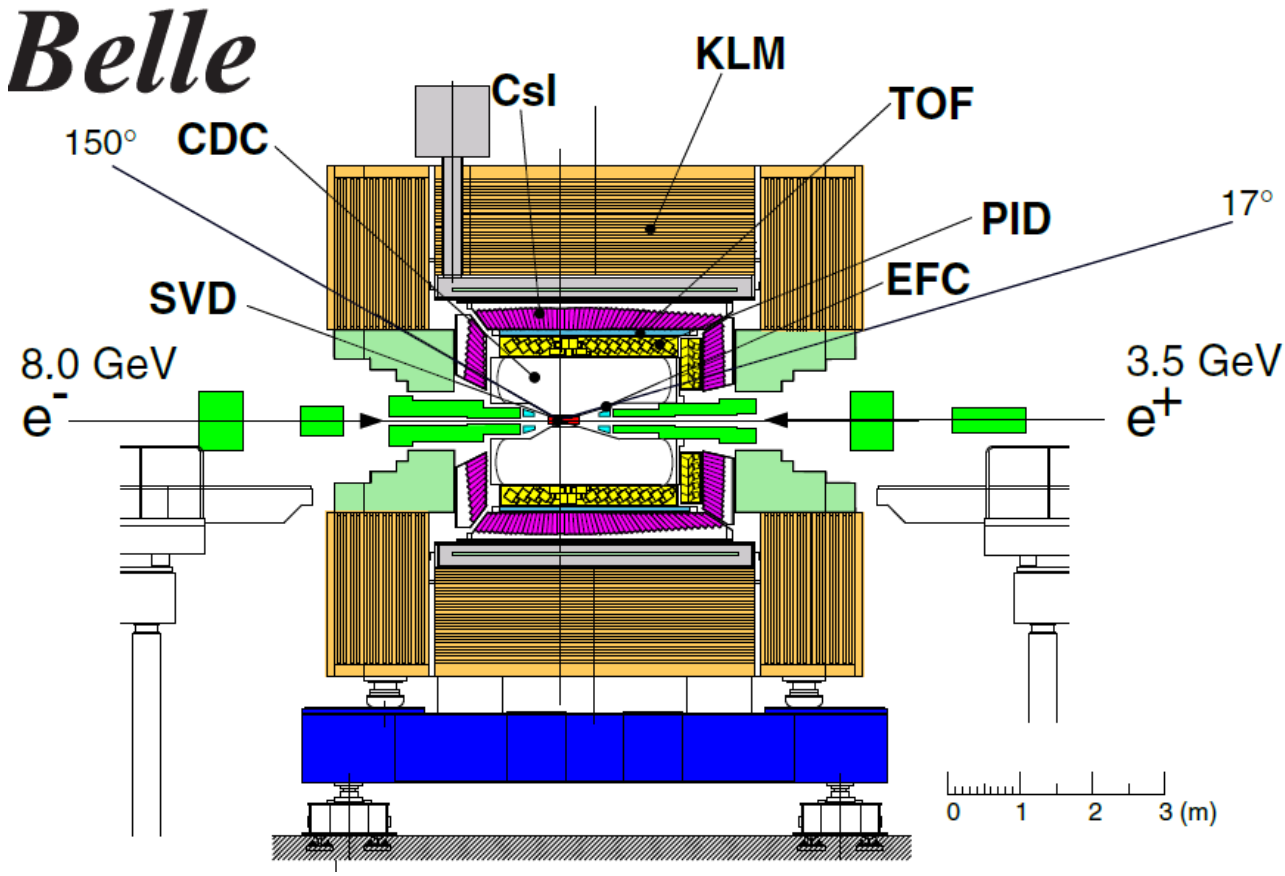

Figure 2.2: The layout of Belle detector.

Beam pipe is the inner most part of the detector and all the particles pass through it before reaching SVD. Double walled Beryllium cylinder is used as a beam pipe for two reasons: it should be such thick as to withstand the beam induced heating and the material should be minimum to avoid Coloumb scattering. The SVD provides precise measurement of the decay vertices of *B* mesons. SVD2 consists of four cylindrical layers whose radii are 20.0 nm, 43.5 nm, 70.0 nm and 88.0 nm. The angular

acceptance is 17° to 150°. The CDC determines the three dimensional trajectories and momenta of charged particles. A superconducting solenoid provides a 1.5 T magnetic field and it bends the charged particle according to their momenta. In addition, CDC measures the energy loss (*dE/dx*) of charged particles. Identification of $\pi^{\pm}$ and $K^{\pm}$ is very important. In the momentum region below 1 GeV/*c*, *dE/dx* measurement from CDC and time of flight measurements are used to perform k/π separations. The ACC provides the K/π separation in momentum range of $1.2 < p < 3.5$ GeV/*c* by detection of the Cherenkov light from particle penetrating through silica aerogel radiator. Time of flight detector system has a time resolution of 100 ps. The counters measure the elapsed time between collision at IP and hitting of particle at TOF layers. From this measured time from TOF and measured flight length and momentum from CDC, one can estimate the mass of each track in the event.

An electromagnetic cascade as pair production and Bremsstrahlung is initiated when a high energy electron or photon is incident on a thick observer, which generates more electrons and photons with lower energy. ECL detects photons with high efficiency and good resolutions in energy and position. Most of the photons are end products of the cascade decays. So ECL should have a good performance below 500 MeV. High energy photons (up to 4GeV) are also produced from some decay modes and high resolution is needed to reduce the background of these modes. The electron is identified using the following information:

- Matching the charged track measured by the CDC and that of the energy cluster measured by ECL.
- Ratio of energy measured by ECL to momentum measured by CDC, *E/p*.
- *dE/dx* in CDC.
- Light yield in ACC.

A charged particle with momentum vector at an angle with respect to the magnetic field will have a helical trajectory. The momentum magnitude can be determined from the radius of curvature of helix. To measure the particle momentum in CDC, 1.5 T magnetic field is applied parallel to the beam pipe. The K^0_L/μ (KLM) detector detect K^0_L mesons and identify muons. It is the only detector which is outside the solenoid magnetic field. K^0_L particles live long so that it will travel beyond ECL. They induce showers of ionizing particles in ECL and it continues to KLM. The position information of K^0_L is provided by the detector. Muons lose their energy

mostly through ionisation process. They penetrate ECL easily and continue through most of all KLM. KLM tracks matching with CDC tracks are identified as muons [9].

Particle	Energy	Momentum	Position	Particle identification
e^- (e^+)	ECL	CDC	SVD, CDC	ECL, ACC, TOF, CDC
μ^- (μ^+)		CDC	SVD, CDC	KLM, ACC, TOF, CDC
π^- (π^+)		CDC	SVD, CDC	ACC, TOF, CDC
K^- (K^+)		CDC	SVD, CDC	ACC, TOF, CDC
p ($\underline{p}$)		CDC	SVD, CDC	ACC, TOF, CDC
γ	ECL		ECL	ECL, CDC
K_L^0			KLM	KLM

Table 2.1: How particle is identified.

Chapter 3

Data Analysis

3.1 Blind Analysis

A blind analysis is a method where one first validates his/her study on the Monte Carlo (MC) simulations, data side-band regions before looking at the data. This way, one can avoid the bias in his/her analysis. As we know that the value of measurement depends upon the cuts one applies and to measure a quantity for the first time, one can tune the cuts on data to artificially increase the significance of his/her study, which is basically a bias. The work done in this thesis is motivated by the "Blind analysis philosophy". Therefore, first we study the signal MC and then background MC. We tried to come up with strategy to reduce the background as much without sacrificing much of the signal.

3.2 Analysis Chart

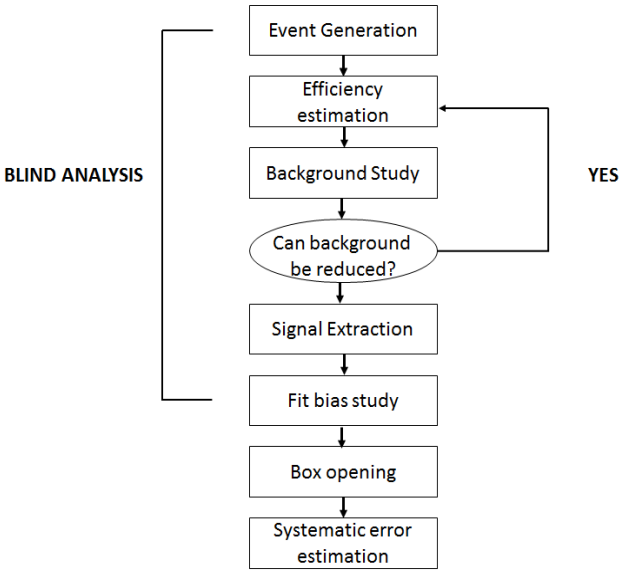

3.3 Event selection

The Belle data consists of a large number of events which not only comes from $e^+ e^- \rightarrow c\underline{c}$ but also from several other processes such as Bhabha, tau pair, continuum events $e^+e^- \rightarrow q\ \underline{q}$ (where q stands for u, d, s, and c), two photons and beam gas interaction, which occur with similar or large cross section than $c\underline{c}$ production. Events with D mesons candidates are selected by applying general hadronic events selection criteria. One of them is, all selected charge tracks are required to satisfy impact parameter cuts: distance of closest approach to the Interaction Point (IP) along with the beam direction $|dz| < 5$ cm and in the x-y plane $|dr| < 2.5$ cm.

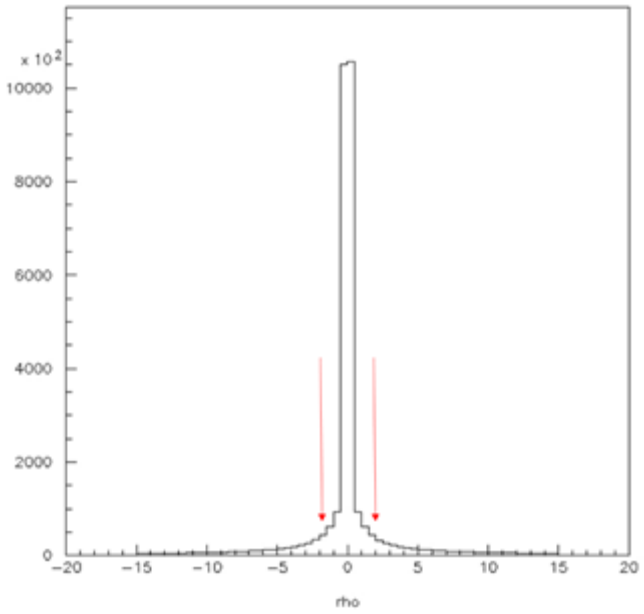

Figure 3.1: This plot shows the *dr* distributions for all the events. We selected the events with -1.5<|*dr*|<1.5 cm cuts (show here with the red arrows).

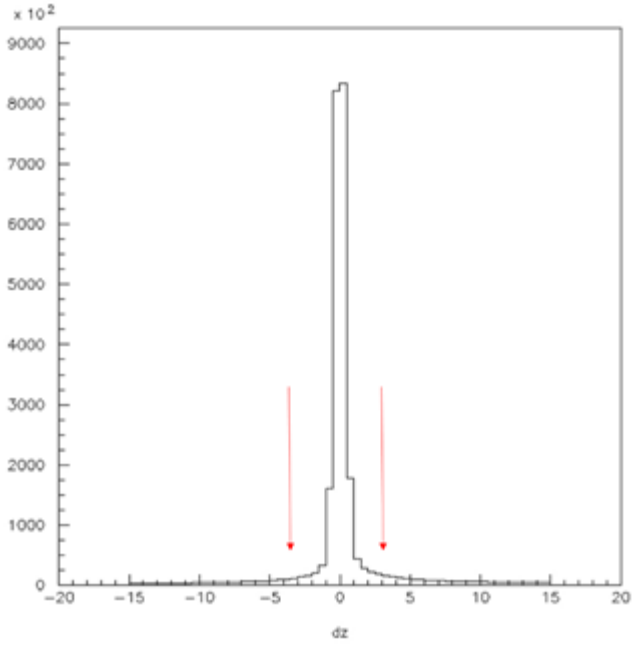

Figure 3.2: This plots shows the *dz* distributions for all the events. We selected the events with -3.5<|*dz*|<3.5 cm cuts (show here with the red arrows).

3.4 Event generation

In MC study, EvtGen is used as an event generator [10]. The generated events are then made to pass through a detector stimulation using GEANT3 package [11]. This package basically accommodates the geometry of each sub-detector components and digitizes the events. To make MC more compatible with data (or in simple term more realistic), randomly selected backgrounds events (which comes from the beam and electronic noise in the detector components) are merged into these generated events. We generated experiment dependent run independent signal MC. Fig 3.3 (taken from J. Wicht slides) explain the procedure done for the MC generation.

Decay files needed as input for the EvtGen are written for each decay mode under study. We generated 1 Million signal events for each decay channel, using the appropriate package available in the EvtGen.

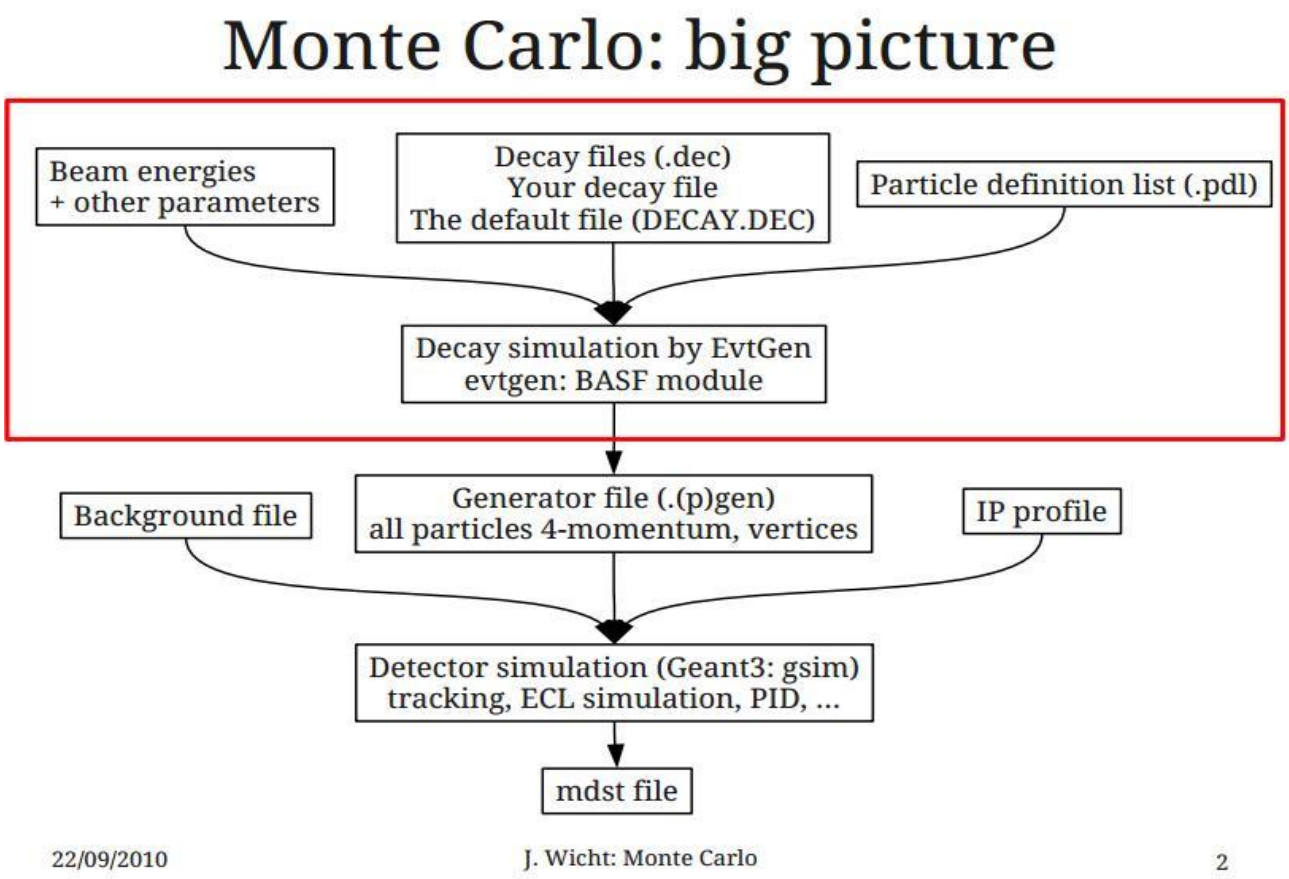

Figure 3.3: This diagram shows the procedure done for generation of the MC simulation events.

3.5 Pion and Kaon Identification

In order to separate K and π, we combine information from ACC, TOF and CDC (dE/dx). From this we basically get likelihood ratio that compares two particles K and π:

$$R(K/\pi) = L(K) / (L(K) + L(\pi))$$

where, L is a product of likelihood from three sub-detectors (i.e. $L = L^{ACC} \times L^{TOF} \times L^{CDC}$). If the value of this term, $R(K/\pi)$ tends to 1 then the charged particle is K-like, and if tends to be 0 then it's a π-like i.e. $R(K/\pi) = 1 - R(\pi/K)$. Please be aware that $R(K/\pi)$ is not a probability to be a kaon. Generally, we apply selection like $R(K/\pi) > 0.6$.

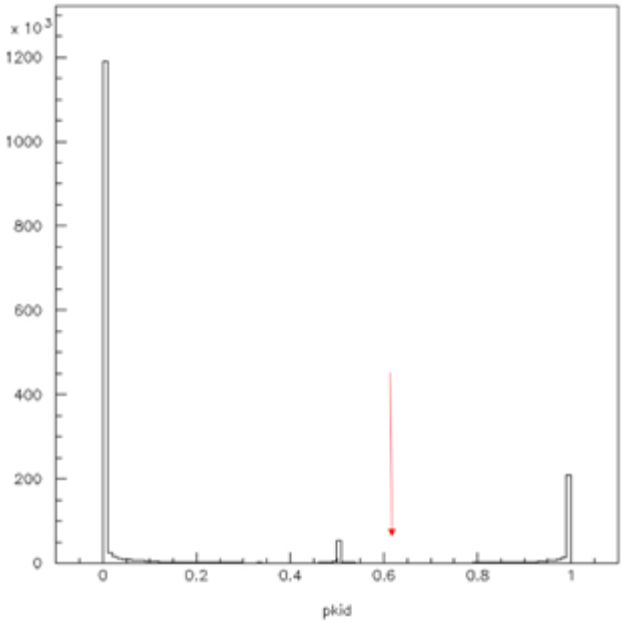

Figure 3.4: This plot shows the distribution for $R_K = (L_K) / (L_K + L_\pi)$. Red arrow shows the value of the cut $R_K > 0.6$ used to select the Kaons candidates for this study.

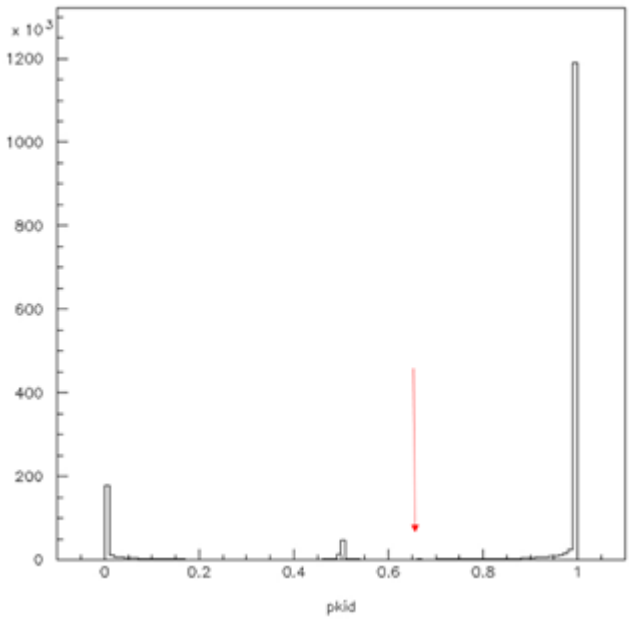

Figure 3.5: This plot shows the distribution for $R_\pi = (L_\pi) / (L_K + L_\pi)$. Red arrow shows the value of the cut $R_\pi > 0.6$ used to select the Kaons candidates for this study.

3.6 Reconstruction of Particles

Using the identified particles, intermediate and final states can be reconstructed.

3.6.1 Reconstruction of ρ

The ρ candidates are reconstructed from its decay mode $\rho^{+} \rightarrow \pi^{0}\,\pi^{+}$. As we know π^{0} decays to two photons with a branching fraction of 98.8 %. In order to reconstruct π^{0}, we combined two γ having energy more than 60 MeV in order to remove the background from fake γs. Further, we selected only those reconstructed π^{0} candidates whose invariant mass fall within 120-150 MeV/c^{2} mass window. The histogram in Fig 3.5 (left) shown below represents the mass of π^{0} and Fig 3.5 (right) represents the reconstruction of ρ by addition of π^{+} in π^{0}.

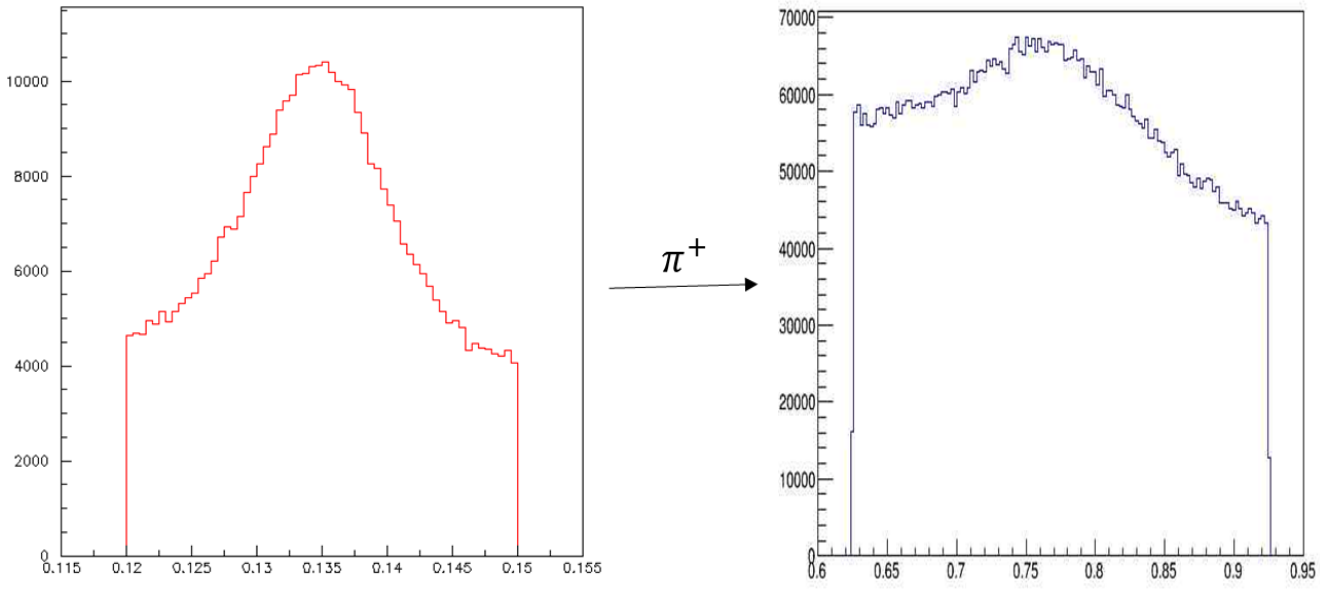

Figure 3.6: (Left) *M(γγ)* invariant mass shows the selected π^{0} candidates. (Right) Invariant mass, $M(\pi^{+}\pi^{0})$, distribution shows the selected ρ events. Both plots are in GeV/c^{2}.

3.6.2 Reconstruction of K^{*}

The K^{*+} is reconstructed from its decay mode $K^{*+} \rightarrow K_S^{0}\pi^{+}$. K_S^{0} decays to π^{+} and π^{-} with a branching fraction of 63.2%. K_S^{0} is reconstructed using two charged π tracks.

Their flight length, angle between the tracks and the decay vertex is exploited in order to avoid fake combinations. Fig 3.5 (left) shows the invariant mass of dipions. We selected K_S^0 candidates having invariant mass within 0.47-0.53 GeV/c^2 and added another charged pion candidate to reconstruct K^{*+}. Fig. 3.5 (right) shows the invariant mass of the reconstructed of K^{*+} by addition of π^+ in K_S candidates.

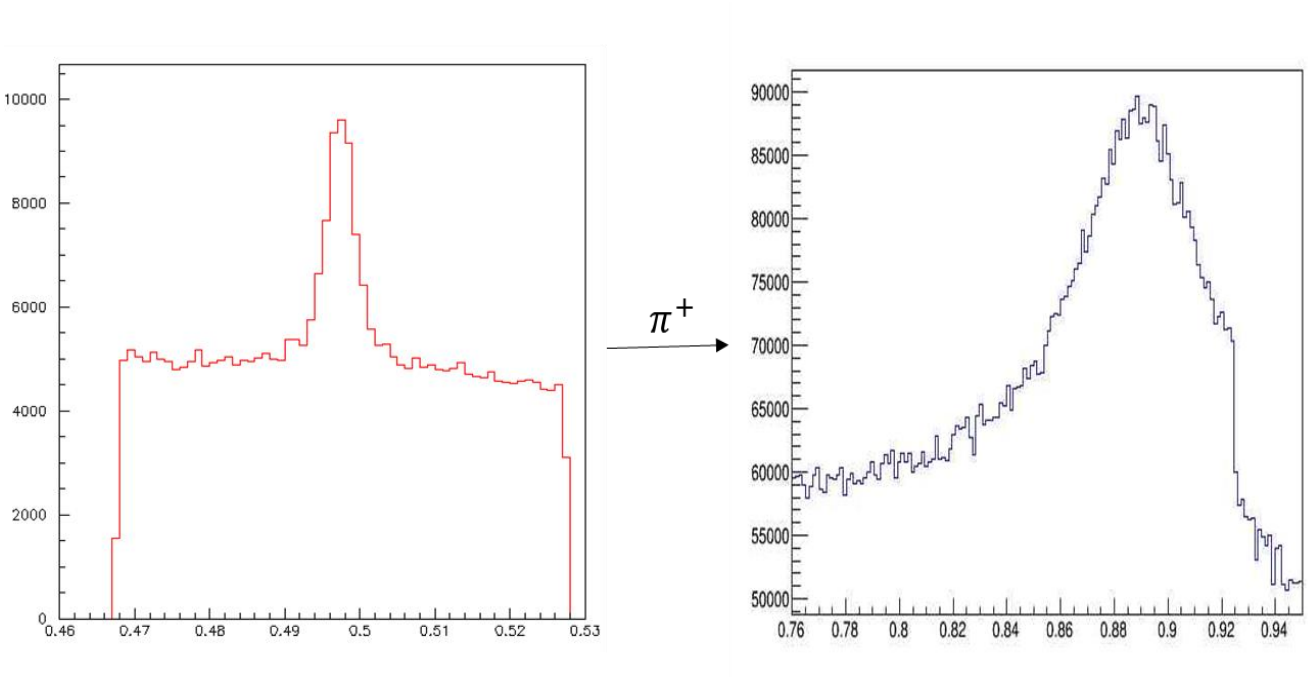

Figure 3.7: (Left) $M(\pi^+\pi^-)$ invariant mass used to reconstruct K_S^0 candidates. (Right) Invariant mass of the charged pion and the selected K_S^0 candidates, $M(K_S^0\pi^+)$, used to reconstruct K^{*+} candidates. Both the plots are in GeV/c^2.

3.6.3 Reconstruction of Ds^* and Ds

As explained earlier, we will reconstruct from $D_S^+ \rightarrow \rho^+\gamma$ and $D_S \rightarrow K^{*+}\gamma$. One can simply combine ρ and K^* with γ and make D_S. However, this is not straightforward due to the high level of the background. Finding the D_S signal events will be difficult in the combinatorial background. In order to improve the signal to noise ratio, we used method called "D_S* tagged identification". We know that $D_S^{*+} \rightarrow D_S^+\gamma$. We exploit the D_S^{*+} and tagged the D_S^+ signal events.

$$D_S^{*+} \rightarrow D_S^+\gamma,$$

$$D_S^+ \rightarrow \rho^+\gamma \text{ or } K^{*+}\gamma$$

From our signal MC data set, we expect the energy of gamma of D_S^* particle, as shown in Figure 3.8. As the difference in their mass is less, one expects the photon to

be soft (which means gamma has low energy). Similarly, we studied the Energy of the photon coming from the D_S radiative decay, shown in Figure 3.9 and as expected its energy is larger than the gamma of D_S*.

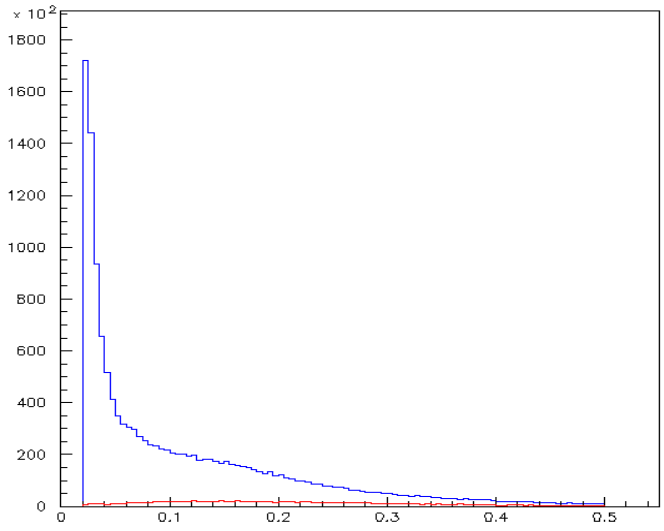

Figure 3.8: Energy of the gammas used in reconstructing the D_S* candidates, The red histogram is the signal, while the blue one is for fake gammas. The plot is in GeV.

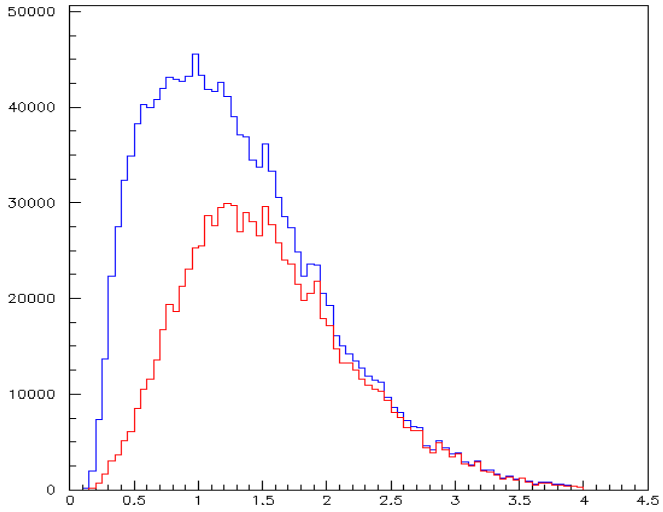

Figure 3.9: Energy of the gammas used in reconstructing the radiative decay of D_S. The red histogram is the signal, while the Blue one is background. The plot is in GeV.

3.6.4 Reconstructed invariant mass of D_s

Figure 3.10 shows the invariant mass of radiative D_S decay generated by us. From this distribution, it is evident that reconstructed D_S contains lot of background. In order to reduce the background, we apply $1.875 < Mass(D_S) < 2.075$ GeV/c^2 cut. This result in reduction of the fake combinations and helps in identifying the signal

Further, we found that most of the fake combinations are due to the photons coming from π^0, Therefore, we applied π^0 veto, it basically rejects the gammas coming from π^0 decay. As see form Figure 3.10 (right), we are able to reduce the background with minimum signal loss.

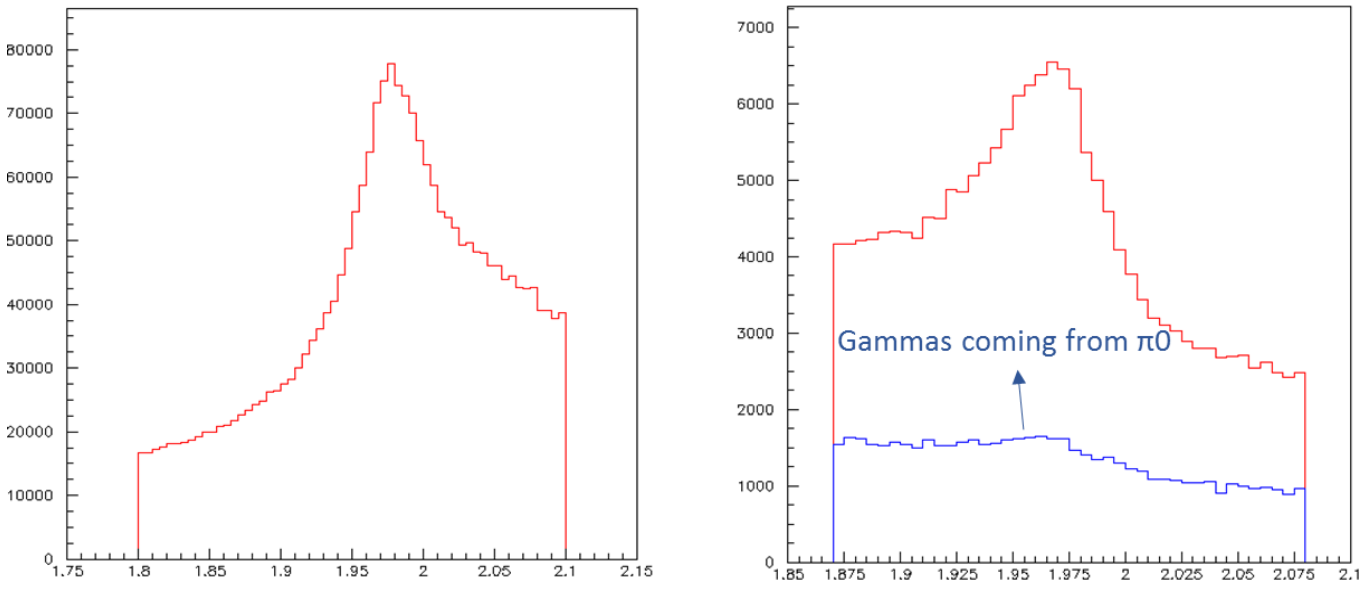

Figure 3.10: (Left) Plot shows the invariant mass of reconstructed D_S particle. $1.875 < \text{Mass}(D_S) < 2.005$ GeV/c^2 is used to identify the D_S signal (Right) Red histogram shows the total events, while the blue histogram shows the background rejected by the π^0-veto. Both plots are in GeV/c^2.

3.6.5 Signal identification (ΔM)

As explained earlier, we are using D_S^* tagging to reduce the background. In order to extract the signal yield, we use

$$\Delta M \equiv Mass(D_S^*) - Mass(D_S).$$

This helps in cancelling the resolution of D_S candidates, which results in better resolution of ΔM. Figure 3.11 (left) shows the ΔM distribution for $D_S \rightarrow \rho\gamma$. Figure 3.11 (right) shows the ΔM distribution in $0.08 < \Delta M < 0.2$ GeV/c^2 range used for the fitting along with the impact of π^0 veto.

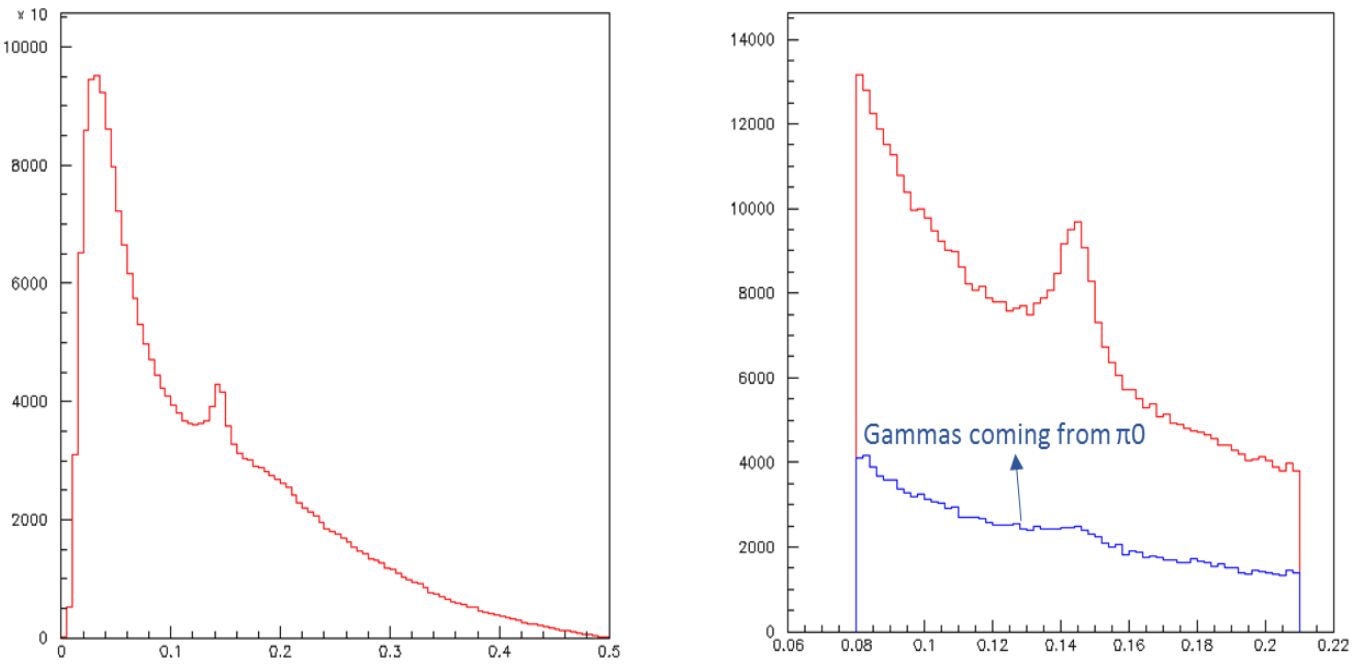

Figure 3.11: (Left) shows the ΔM distribution for $D_S \rightarrow \rho\gamma$. (Right) Shows the ΔM distribution in the range which will be used for signal fitting. Blue color shows the background rejected using the π^0 veto.

3.6.6 *Mass(D_S)* vs ΔM

Fig. 3.12-3.14 shows the *Mass(D_S)* and ΔM in 2D plot. One can see how the signal peaks in both. However, the signal is narrower in ΔM (as expected) in comparison to *Mass(D_S)*. Further, the combinations due to fake gammas are easily separated in ΔM in comparison to *Mass(D_S)*. Fig 3.13 demonstrates the reduction of fake combinations in both dimensions after one applies π^0 veto. In order to see how the true signal behaves, we tag the generated samples using the MC PDG codes for the particles. We matched mothers, grandmothers, and great grandmothers in order to check the true combinations. Fig. 3.14 is the plot for the true candidates (after removal of fake combinations after matching the MC PDG codes). Using which, we verify that ΔM is a better variable to identify the signal.

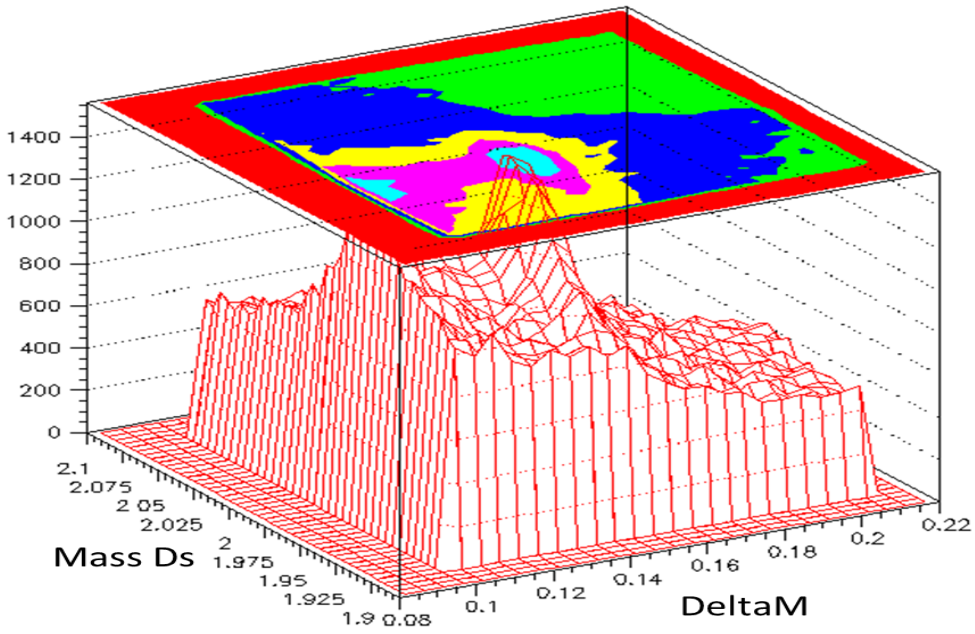

Figure 3.12: *Mass(D_S)* and ΔM distribution for all the reconstructed combinations in the signal MC after all the cuts and criteria is applied.

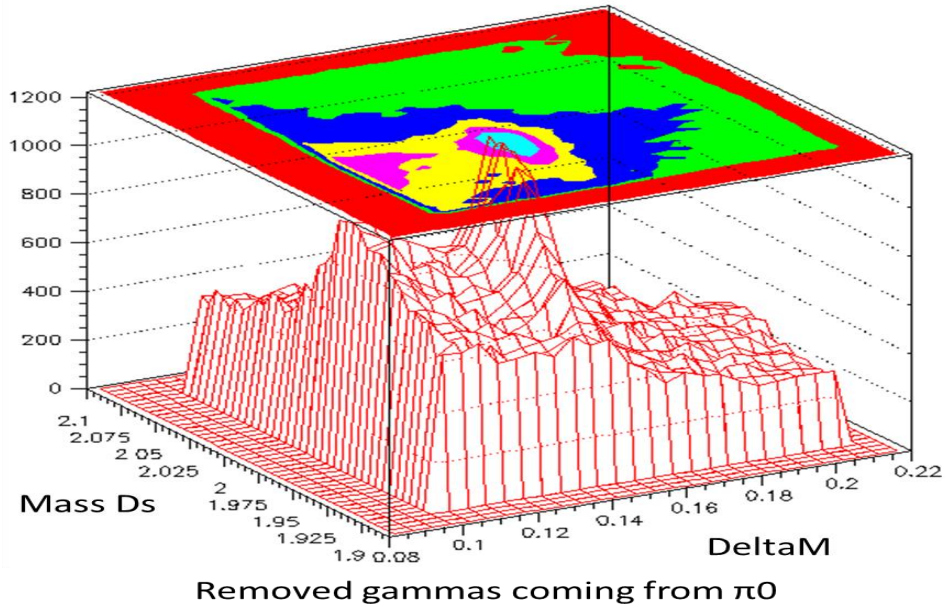

Figure 3.13: *Mass(D_S)* and ΔM distribution after π^0 veto is applied

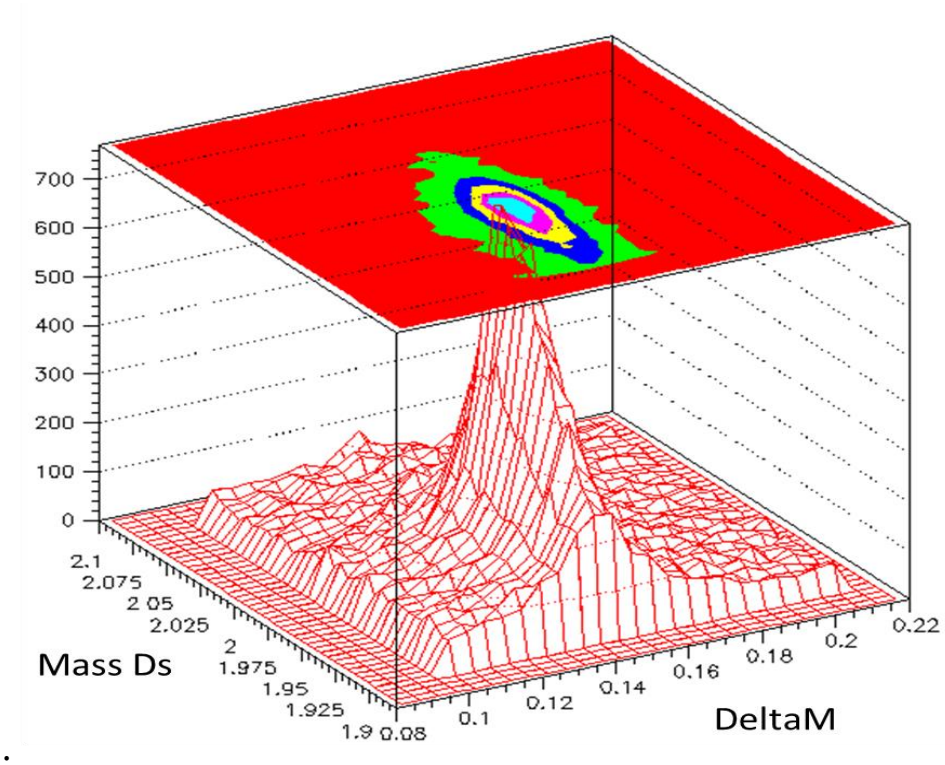

Figure 3.14: *Mass(D_S)* and ΔM distribution for the MC truth matched signal i.e. pure signal.

3.7 Skim

Skim is a subset of data set in which signal purity is enhanced without loss of signal events. Belle detector records wide variety of physics events including *BBbar*, *charm (ee → cc̄)*, tau pair, two-photons, etc. Most of the data is stored in mdst format. In order to efficiently work, one can produce a subset of the data by skimming the full data-sets.

3.7.1 What is skim file?

It is known that analysing whole datasets by individuals is inefficient as it takes much time and occupies large disk space. Therefore, some datasets, in which the specific physics mode is enhanced, is prepared for Belle Physicists. However, the decay mode of our interest is not in those skims. I worked on production of the skim files for our decay modes of interest. For which, we wrote a skimming module and run on all the generic MC sample and the date.

Generic MC sample is divided into four types:

1) ***uds*** : This sample has uu^{bar}, dd^{bar} and ss^{bar} production at the $\Upsilon(4S)$ energy, which further fragments into the pion, kaons or protons.

2) ***charm*** : This sample has cc^{bar} production. We are more interested in this, as it contain $D_{(s)}^{(*)}$ mesons. We expect to have most of the background from this sample.

3) **Charged** : Charged *B* decays are included in this sample. Almost all the known or expected decay modes of charged *B* are produced in this sample.

4) **Mixed** : Neutral *B* decays are included in this sample. Here also, all the known or expected neutral *B* decays are produced in this sample.

   For now, I concentrate on charm, charged and mixed sample to study the background. As, we expect to have D_S decays in cc^{bar} and *B* decays.

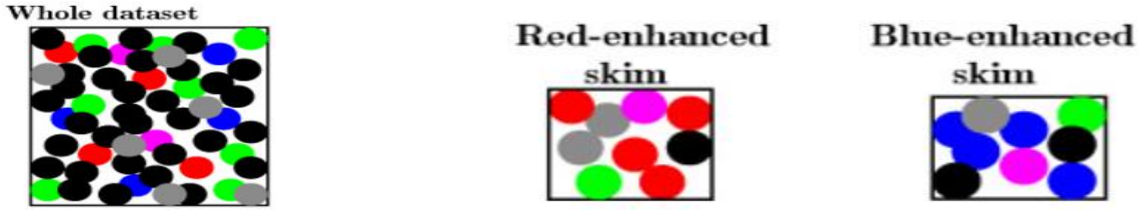

Figure 3.15 The box on the left shows the whole dataset, where color ball refers to the different events. The box in the center and right shows the red-enhanced and blue-enhanced skimmed sample, respectively. This suggest what skim means.

The procedure carried to produce the skimmed index files.

1) Run on the whole data and generic MC samples.

2) Identify the signal modes by applying loose cuts and criteria.

3) If we find some signal, we save the index file for that particular event.

4) Index files are basically pointers to a particular event number, run number and the experiment number.

5) In end, we have index files which can be used to analyse the data set or generic MC. These index files are smaller and are faster. This helps in saving time and computational power.

3.8 ΔM in Signal and Background MC

3.8.1 Signal MC

Figure 3.14 shows the ΔM distribution for $D_S^+ \rightarrow \rho^+\gamma$ decay mode for signal MC after all the cuts and criteria are applied. One can clearly see the signal. However, still there is lot of combinatorial background which is flat. In an attempt to further decrease the combinatorial background, we studied p_{Ds}* which is the momentum of D_S^* in the centre-of-mass frame. As shown in the Figure 3.15, one can remove the combinatorial background. As, we expect the D_S^{*+} to come from cc^{bar} production, its p_{Ds}* is expected to have large value. Different cuts on p_{Ds}* was studied and we found cut at p_{Ds}* > 2.0 GeV/c to be the optimum cut where signal loss is less. At this cut, we expect signal loss of 23% in comparison to background reduction by 75%. Due to which, we choose to apply further condition of p_{Ds}* > 2.0 GeV/c.

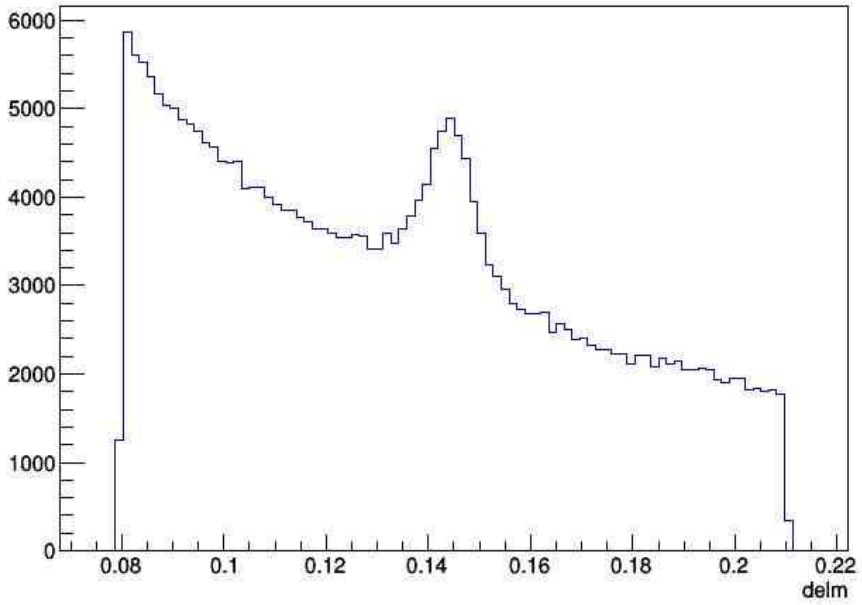

Figure 3.14: Distribution for the ΔM in the signal MC sample after all the cuts and criteria explained till now. Still, the combinatorial background seems to be huge.

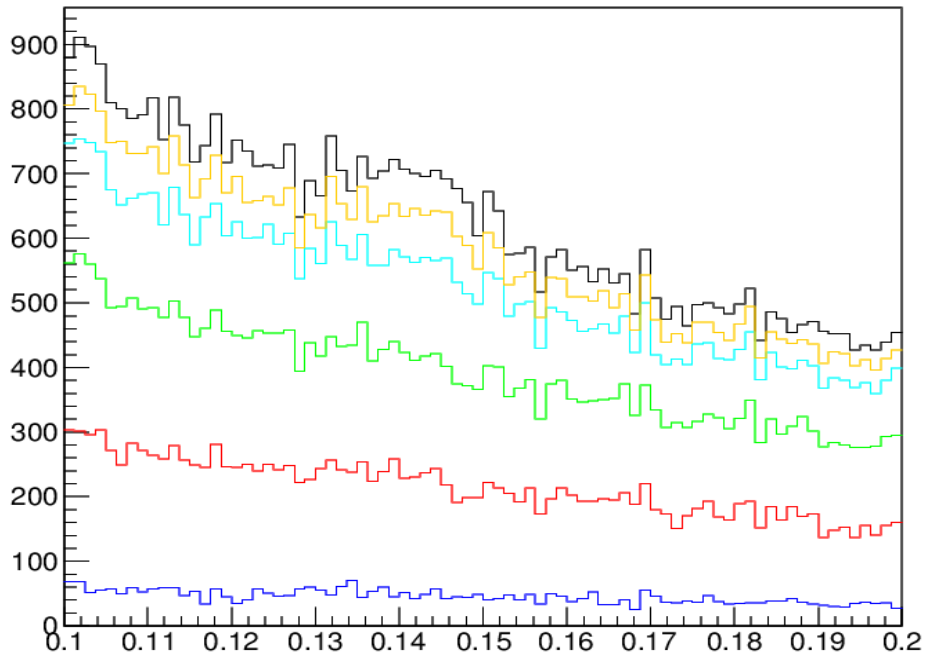

Figure 3.15: This histogram shows variation in ΔM for different values of p_{Ds}^*, which is the momentum of D_S^* in the centre-of-mass frame. Blue, red, green, cyan, yellow and black are the ΔM distribution for p_{Ds}* to be less than 0.5 GeV/c, 1.0 GeV/c, 1.5 GeV/c, 2.0 GeV/c, 2.25 GeV/c and 2.5 GeV/c, respectively. As seen, after the cut at p_{Ds}* < 2.0 GeV/c, we start having some signal component. So, we choose p_{Ds}* > 2.0 GeV/c in order to avoid combinatorial background.

Figure 3.16 (left) shows the final ΔM distribution for the $D_S^+ \rightarrow \rho^+\gamma$. As one can see, the signal is more prominent here. Now, in order to extract the signal, we perform an unbinned maximum likelihood (UML) fit using RooFit. The PDF used for the fit is

$$\mathcal{L} = \frac{e^{-N}}{N!}\prod_{i=1}^{N}\{bkg \times Polynomial(\Delta M; slope1, slope2, slope3) + sig \times (Sum\ of\ Two\ Gaussian)(\Delta M; mean, sigma1, s2s1, a2a)\}$$

Here, *bkg* is the events estimated for the background, while *sig* are the events estimated for the signal. Further, Sum of Two Gaussian is defined as follows:

$$Sum\ of\ Two\ Gaussian = (1 - a2a)Gaussian(Mean, Sigma1) + a2a\ Gaussian(Mean, Sigma1 \times s2s1)$$

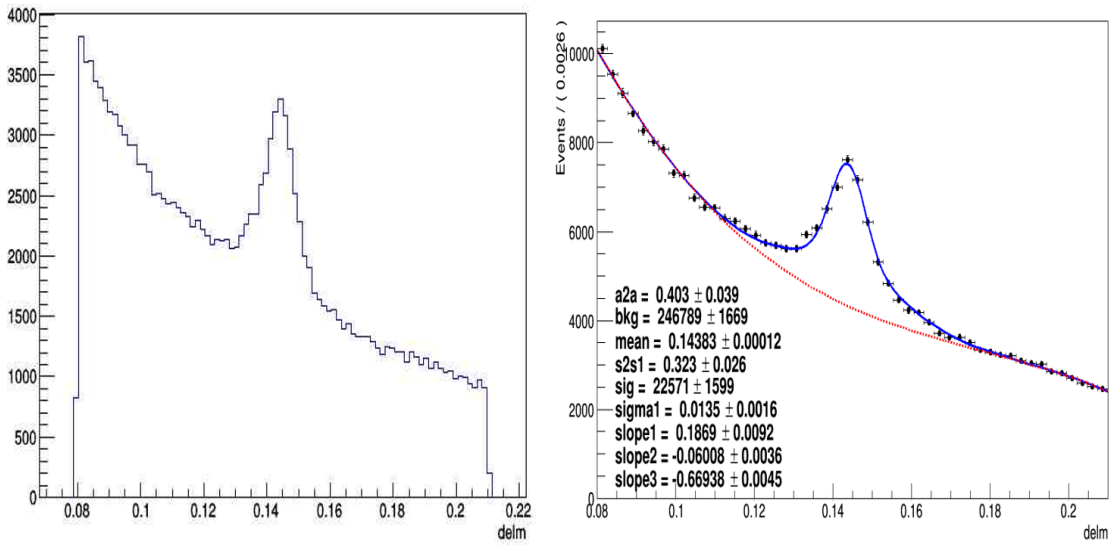

Figure 3.16: (Left) Shows the ΔM distribution for the signal after applying p_{Ds}* cut. (Right) Shows the UML fit to the ΔM distribution.

Using the UML fit, we expected the signal efficiency to be 2.3%. Further, in order to verify our understanding that we are not removing much of our signal if we apply p_{Ds}* cut. We perform UML fit to the rejected events, after fixing the parameters estimated from the fit to the Figure 3.17. As seen in Figure 3.17, the signal lost is small as compared to the background reduction.

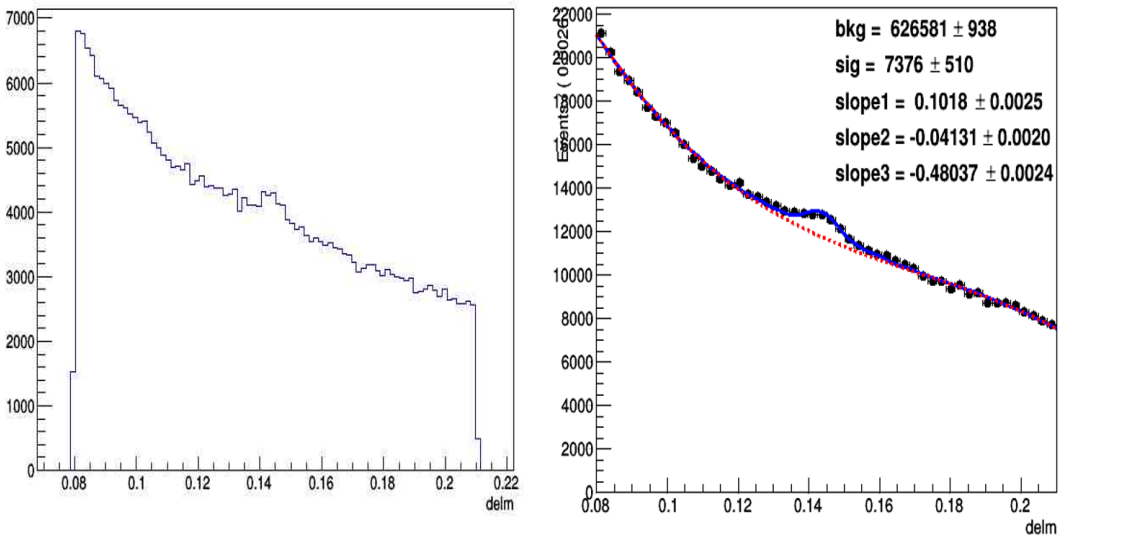

Figure 3.17: (Left) shows the ΔM for the p_{Ds}* < 2.0 GeV/c. (Right) shows the UML for to the ΔM distribution for p_{Ds}* <2 .0 GeV/c

3.8.2 Background MC

As explained earlier, we studied the background for our data using three main sources:

1) cc^{bar}
2) Charged B decays.
3) Mixed B decays.

We expect most of the background to come from the cc^{bar}. Figure 3.18 and Fig 3.19 where all the three backgrounds are stacked for the p_{Ds}* and ΔM distributions.

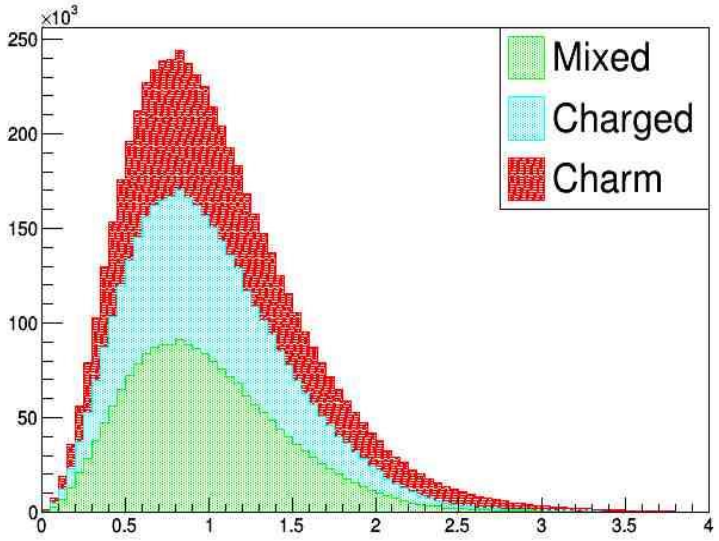

Figure 3.18: This p_{Ds}* distribution is for all the backgrounds one can expect.

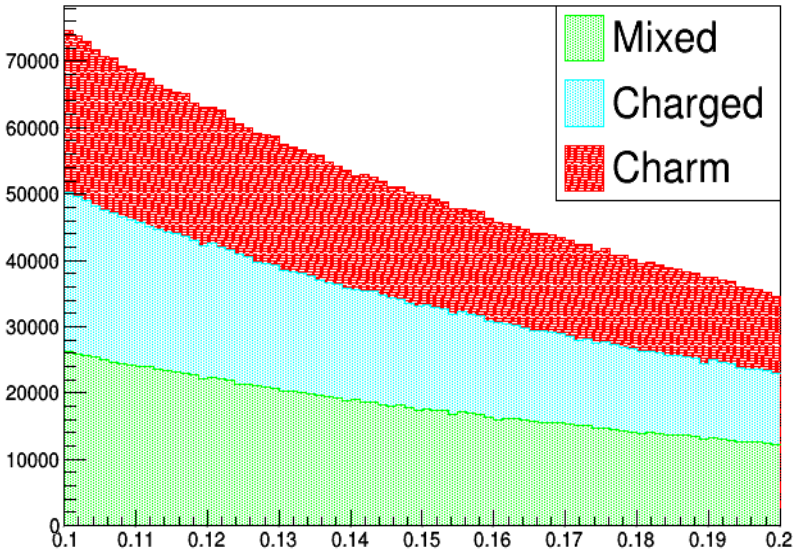

Figure 3.19: ΔM distribution without p_{Ds}* cut for background modes.

Here we also studied the p_{Ds}* for each source and found that our p_{Ds}* cut is able to

reduce most of them. As demonstrated in Fig. 3.20, most of the background gets removed by the p_{Ds}* < 2.0 GeV/c cut.

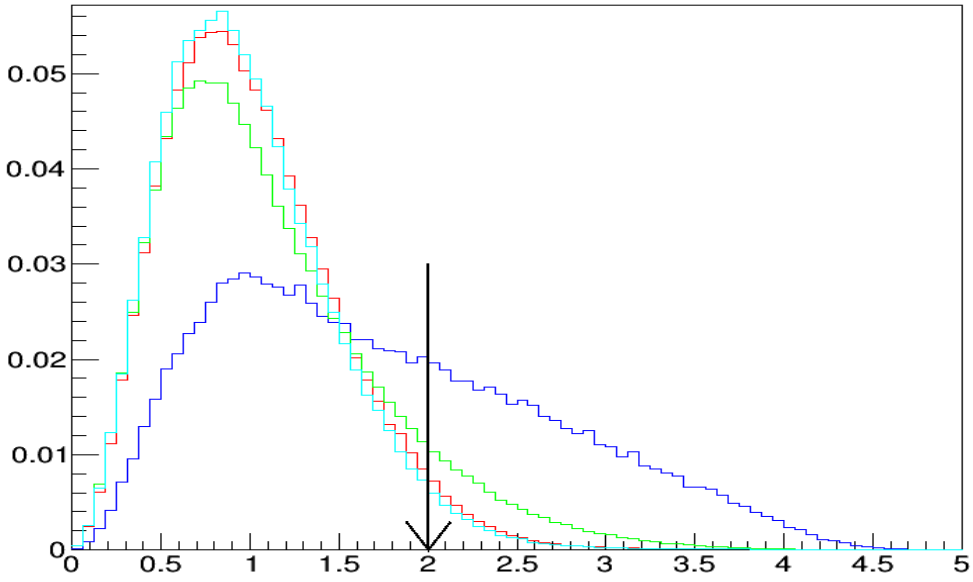

Figure 3.20: The distribution shows p_{Ds}* distribution for signal (blue), c$\underline{c}$ (red), Cyan (charged) and Red (mixed). We can easily conclude that after 2.0 GeV/*c* there is more signal whereas for the value less than 2.0 GeV/*c* we have mostly background and fake combinations.

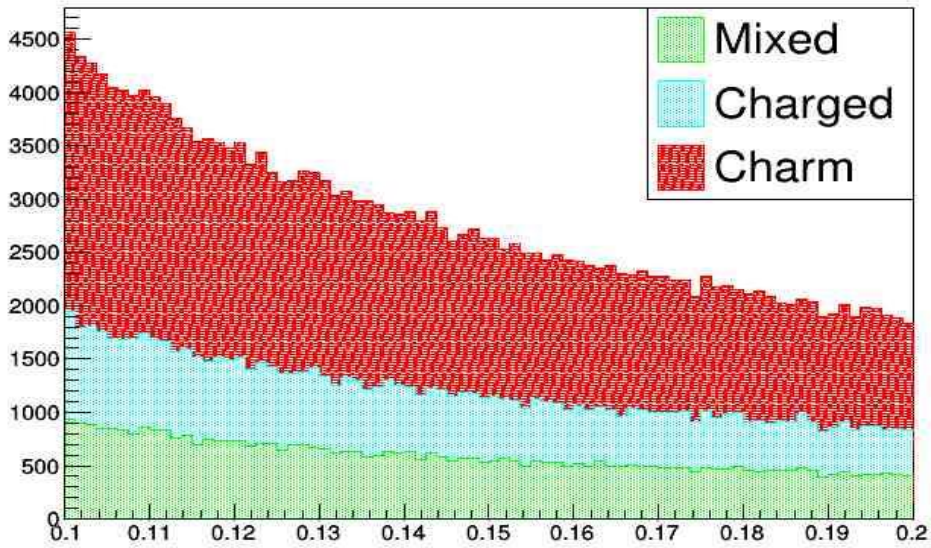

Figure 3.21: ΔM distribution with p_{Ds}* > 2.0 GeV/*c* cut for background modes.

Figure 3.21 shows the stacked plots for the background after applying the p_{Ds}* > 2.0 GeV/c cut. One sees drastic reduction in the background from the Charged and mixed. Which one can explain based on the available momentum. As, the reconstructed D_S is coming from B decays, its momentum in CM frame is expected to be less than 2.0 GeV/c. Most of the background is coming from charm which is again expected as it also contains our signal. However, the good thing is that there is no peaking background is expected.

The knowledge learnt in this study can further be used to optimize the π^0-veto, $Mass(D_S)$ and p_{Ds}*.

Summary

Reconstruction code was prepared for the $D_S \rightarrow \rho\ \gamma$ and $D_S \rightarrow K^*\ \gamma$, where further D_S is used to reconstruct $D_S^* \rightarrow D_S\gamma$ decay modes.

Signal MC was generated for the decay mode of interests using EvtGen and Geant simulation.

Studied different variables and tools in order to suppress the background coming from the random combinations and found that π^0 veto and p_{Ds}^* cuts are effective in reduction of the random combinations.

Prepared skim modules and index files for the generic MC and data. In future, these index files can be used to study and further optimize this study.

For background study, generic MC: charm, charged and mixed sample was studied. The cuts used to reduce random combinations were also effective here to reduce the background.

Probability distribution functions (PDF) was written for unbinned maximum likelihood fit, and fit to signal PDF was done. The signal efficiency was found to be 2.3%.

One can extend this analysis by optimizing the cuts studied here and use the skimmed index files to save time and computational power. We didn't run on data, as it is beyond the scope of this project.

Appendix

Example of typical decay file written in EvtGen used for generating the signal MC.

```
JetSetPar PARJ(21)=0.28

JetSetPar PARJ(25)=0.27

JetSetPar PARJ(26)=0.12

JetSetPar PARJ(33)=0.3

JetSetPar PARJ(41)=0.32

JetSetPar PARJ(42)=0.62

JetSetPar PARJ(81)=0.38

JetSetPar PARJ(82)=0.76

JetSetPar PARP(2)=4.0

JetSetPar MSTP(141)=1

JetSetPar MSTP(171)=1

JetSetPar MSTP(172)=1

JetSetPar MSTJ(11)=4

JetSetPar PARJ(46)=1.0


Alias MyDs+ D_s+

Alias MyDs- D_s-

ChargeConj MyDs+ MyDs-


Alias MyK*+ K*+

Alias MyK*- K*-

Alias MyK_S0 K_S0
```

```
Decay vpho
#       d u s c b t   e   mu  tau
1.0 PYCONT 0 0 0 1 0 0   0 0 0 0 0 0;
Enddecay
Decay D_s*+
1.0 MyDs+  gamma PHOTOS VSP_PWAVE;
Enddecay
Decay D_s*-
1.0 MyDs- gamma PHOTOS VSP_PWAVE;
Enddecay
Decay MyDs+
1.0 K*+ gamma PHOTOS PHSP;
Enddecay
Decay MyK*+
0.99955 pi+ MyK_S0 PHOTOS VSS;
Enddecay
Decay MyDs-
1.0 MyK*- gamma PHOTOS PHSP;
Enddecay
Decay MyK*-
0.99955 pi- MyK_S0 PHOTOS VSS;
Enddecay
Decay MyK_S0
1.0000 pi+ pi- PHOTOS PHSP;
Enddecay

End
```

Bibliography

[1] R. Oerter (2006). The Theory of Almost Everything: The Standard Model, the Unsung Triumph of Modern Physics (Kindle ed.). Penguin Group. p 2. ISBN 0-13-236678-9.

[2] J.D. Lykken, "Beyond the Standard Model". CERN Yellow Report. CERN. **101–109**. arXiv:1005.1676 . CERN-2010-002 (2010).

[3] M.S. Sozzi (2008a). "Parity". Discrete Symmetries and CP Violation: From Experiment to Theory. Oxford University Press. **15–87**. ISBN 0-19-929666-9.

[4] http://hyperphysics.phy-astr.gsu.edu/hbase/Particles/dmeson.html

[5] B. Bajc and S. Fajfer. *Phys. Rev. D* **54**, 5883, 1996

[6] I. I. Bigi, F. Gabbiani, and A. Masiero, *Z. Phys. C* **48**, 633 1990.

[7] I. I. Bigi, Report No. CERN-TH.7370/**94**; Report No. UND-HEP-94-BIG08, hep-ph/9408235

[8] I. I. Bigi, Report No. UND-HEP-95-BIG08, hep-ph/9508294

[9] http://belle.kek.jp/

[10] D.J. Lange, *Nucl. Instrum. Methods Phys. Res sec A* **462**, 152 (2001)

[11] R.Brun et al. GEANT 3.21, CERN DD/EE/**84**-1, 1984